To cite this article: JIANG S C, XU B, WANG Z H. Numerical simulation analysis of liquid sloshing in tank under random excitation [J/OL]. Chinese Journal of Ship Research, 2022, 17(2). http://www.ship-research.com/en/article/doi/10.19693/j.issn.1673-3185.02183.

DOI: 10.19693/j.issn.1673-3185. 02183

Numerical simulation analysis of liquid sloshing in tank under random excitation

JIANG Shengchao[*1], *XU Bo*[2], *WANG Zihao*[1]

1 School of Naval Architecture Engineering, Dalian University of Technology, Dalian 116024, China

2 Marine Design and Research Institute of China, Shanghai 200011, China

Abstract: [**Objectives**] This paper studies the transient effects, different frequencies of spectral peaks, and meaningful excitation amplitudes on liquid sloshing in tank. [**Methods**] A numerical model is established using the computational fluid dynamics (CFD) method, and the reliability of the numerical model is validated through comparison with the analytical solution of linear potential flow and experimental data. [**Results**] The transient effects of random excitation have a significant influence on the fluctuation of the free water surface of liquid sloshing in the tank. By applying the buffer function, stable results can be obtained quickly. When the peak frequency of the excitation spectrum is close to the natural frequency of the tank, the energy of the waveheight response spectrum of the liquid sloshing in the tank is mainly concentrated at the natural frequency of the tank. When the peak frequency of the excitation spectrum is far from the natural frequency of the tank, the energy of the wave-height response spectrum is concentrated near the peak frequency. With the increase in the meaningful amplitude of the excitation spectrum, the amplitude deviation of the liquid sloshing in tank response relative to the linear wave (the deviation degree is zero) increases, and the nonlinearity of the liquid tank increases significantly. [**Conclusions**] For the random excitation simulation, especially when the excitation frequency is far from the natural frequency, it is necessary to buffer the excitation duration. It is found that when the peak frequency of the excitation spectrum moves away from the first natural frequency to higher frequencies, the energy is dominant at the *i*-th order of the natural frequency when the peak frequency is close to it.

Key words: liquid sloshing in tank; random excitation; transient effect; numerical simulation

CLC number: U661.1

0 Introduction

Sloshing is a very common fluid motion that typically occurs in tanks containing liquids, such as those of sailing tankers. Violent liquid sloshing is highly likely to occur in a tank when the frequency of the external excitation is close to the natural oscillation frequency of the liquid, or when the amplitude of the excitation is huge. The sloshing further results in a high impact pressure on the bulkhead or tank roof, ultimately leading to structural damage. Sloshing also has significant small-scale effects, for example, impact pressure and mechanical energy dissipation caused by gas-liquid mixtures, fluid viscosity, and vortex flow. In addition, close coupling between liquid sloshing and ship motion is also likely to take place. Therefore, understanding the fundamental principles of liquid sloshing in tanks is of great importance for offshore operations and structural safety.

Received: 2020 − 11 − 15 **Accepted**: 2021 − 03 − 05

Supported by: National Natural Science Foundation of China (51909027); Fundamental Research Funds for Central Universities (DUT21LK12)

Authors: JIANG Shengchao, male, born in 1984, Ph.D., associate professor. Research interest: interaction between waves and marine engineering structures. E-mail: jiangshengchao@foxmail.com

XU Bo, male, born in 1995, master degree

WANG Zihao, male, born in 1998, master degree candidate. Research interests: interaction between waves and marine engineering structures. E-mail:1429483251@qq.com

***Corresponding author**: JIANG Shengchao

In the aspect of theoretical research, Faltinsen [1] proposed a nonlinear analysis approach for a third-order sloshing model based on the potential flow theory, and this approach took into account the nonlinear effect of the large amplitude motion of the tank. Faltinsen and Timokha [2] refined a semi-analytical method of solving the nonlinear liquid sloshing in a rectangular tank of a finite depth. Zhang et al. [3] studied the second-order sloshing in a three-dimensional tank under surge-sway coupling excitation on the basis of the potential flow theory and perturbation expansion. They derived a theoretical analytical solution and found that second-order resonance would occur when the sum-frequency or difference-frequency of any two excitation components was equal to one of the natural frequencies. The rapid development of high-speed computers and the maturity of computational fluid dynamics (CFD) technologies provide a new and efficient approach, namely, numerical simulation, for studying sloshing motion. Kim [4] developed a finite-difference model to predict the emergence of two- and three-dimensional tank impact and simulated impact in a special buffer zone near the tank top. Besides, a single-valued function was employed to track the sloshing interface. Then, Kim et al. [5] modified the model by extending the buffer zone to the slope boundary near the tank top, reducing the sensitivity of previous models to mesh resolution and time increments. Biswal et al. [6] investigated the nonlinear sloshing response of the liquid in a two-dimensional rectangular tank with a rigid baffle by a finite-element method. Lu et al. [7] studied the liquid sloshing in a rectangular tank with/without baffles and built a viscous fluid model based on a non-inertial reference system. The simulation results showed that the sloshing responses in tanks with/without baffles were both significantly affected by the dissipation effect. Although sloshing response components associated with natural frequencies can eventually be dissipated by damping due to physical dissipation, they are completely retained in the analytical solution of the potential flow, which explains the general overestimation of the sloshing amplitude by the potential flow theory. Liu and Lin [8] investigated the viscous damping effect during the liquid sloshing in a tank with a three-dimensional numerical two-phase flow model. Xiao et al. [9] studied the characteristics of liquid sloshing in a tank under rolling excitation with a numerical viscous flow model that integrated multi-tank liquid sloshing with ship motion and proposed a simplified two-dimensional multi-tank model.

Most of these studies focus on regular excitation, and those investigating liquid sloshing in a tank under random excitation are scarce. Nevertheless, compared with regular excitation, random excitation is more analogous to sea waves and so on in terms of irregular action on a tank. On the basis of outlining and applying a numerical viscosity model and the principles of random excitation, this study intends to investigate the transient effect and temporal sensitivity in the case of liquid sloshing in a tank under random excitation, as well as the influences of spectral peak frequency and amplitude on sloshing characteristics under random excitation.

1 Principles and numerical methods

This study mainly resorted to the software STAR-CCM+ for the numerical simulation of liquid sloshing in a tank under forced excitation. Considering the incompressible viscous two-phase flow involving mesh motion, the Navier-Stokes (N-S) equation leveraging an arbitrary Lagrangian-Eulerian (ALE) method is as follows:

$$\frac{\partial \rho u_i}{\partial x_i}=0 \tag{1}$$

$$\frac{\partial \rho u_i}{\partial t}+\frac{\partial\left(\rho(u_i-u_i^{\mathrm{m}})u_j\right)}{\partial x_j}=-\frac{\partial p}{\partial x_i}+\mu\frac{\partial}{\partial x_j}\left(\frac{\partial u_i}{\partial x_j}+\frac{\partial u_j}{\partial x_i}\right)+f_i \tag{2}$$

where ρ is the fluid density; x_i and x_j are the displacement components in the i and j directions, respectively; u_i and u_j are the velocity components in the i and j directions, respectively; u_i^{m} is the velocity of the mesh motion, that is, the velocity component in the i direction; t is time; μ is the fluid dynamic viscosity coefficient; f_i is the body force on per unit volume of fluid, it was gravity alone in this study and thus set to 9.81 m/s^2.

In order that the model can meet the simulation requirements in the case of wave breaking, this paper employed the volume of fluid (VOF) method to capture the movement of the free water surface. The fluid phase function φ was defined as follows:

$$\varphi=\begin{cases}\varphi=0, & \text{in air}\\ 0<\varphi<1, & \text{on free surface}\\ \varphi=1, & \text{under water}\end{cases} \tag{3}$$

It satisfied the following boundary equation in the framework of the ALE method:

$$\frac{\partial \varphi}{\partial t}+(u_i-u_i^{\mathrm{m}})\frac{\partial \varphi}{\partial x_i}=0 \tag{4}$$

Then, the density and dynamic viscosity coefficient distributions of the two-phase flow were determined:

$$\rho = \varphi\rho_{\mathrm{w}} + (1-\varphi)\rho_{\mathrm{a}}$$
$$\mu = \varphi\mu_{\mathrm{w}} + (1-\varphi)\mu_{\mathrm{a}} \tag{5}$$

where ρ_{w} and ρ_{a} are the densities in water and air, respectively; μ_{w} and μ_{a} are the dynamic viscosity coefficients in water and air, respectively. In data processing, the contour of φ = 0.5 was set as the free water surface of the liquid.

The finite volume method (FVM) was used to discretize the control equations (Eqs. (1) to (2)) and the boundary equations (Eq. (4)) of the two-phase flow. Specifically, the time discretization was in the Eulerian format, the scatter and gradient were in the Gauss Vanleer and Gauss linear formats, respectively, and the diffusion term was in the Gauss linear corrected format. The N-S equations were solved by the pressure implicit with splitting of operators (PISO) method [10], where the velocity equation could be solved directly by algebraic methods and the pressure equation was solved iteratively by the BI-CGSTAB [11] method. During calculation, the point in the top lid of the container was used as the reference pressure point and set to zero Pa.

In the numerical calculation, the time step selected should satisfy the Courant-Friedrichs-Lewy (CFL) condition (Eq. (6)), and it can be automatically selected according to the Krone number Cr.

$$\Delta t < \min\left\{\frac{Cr\times\Delta x}{u_{\max}}, \frac{Cr\times\Delta y}{v_{\max}}, \frac{Cr\times\Delta z}{w_{\max}}\right\} \tag{6}$$

where $u_{\max}$, $v_{\max}$, and $w_{\max}$ are the maximum velocity components in the x, y, and z directions, respectively. In calculation, the CFL condition can be met in principle when Cr is set to 1.0. In this study, Cr was set to 0.20 to assure computational precision when the free water surface was in large-amplitude nonlinear motion.

2 Verification of numerical model

The above numerical model was used to study the liquid sloshing in a rectangular tank under horizontal excitation. The numerical model was divided into 25 000 meshes, and the areas near the free liquid surface and the bulkhead were set as densified areas. The minimum and maximum sizes of the meshes are 5 mm and 10 mm, respectively. The liquid sloshing in a rectangular tank with width W=1 m and loading depth d = 0.5 m was numerically simulated to verify the validity of the model. In this case, the self-oscillation frequency of the liquid sloshing in the tank was ω_0 = 5.316 rad/s. As shown in Fig. 1, the tank was subjected to sinusoidal excitation.

$$x = A\sin\omega t \tag{7}$$

where A is the excitation amplitude; ω is the excitation frequency.

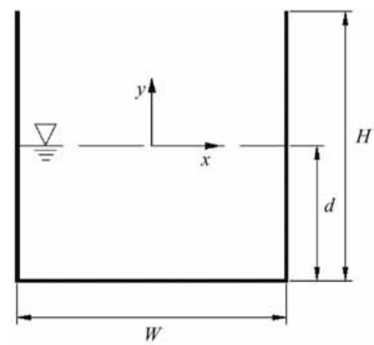

Fig. 1 Geometric model of rectangular tank

The analytical solution proposed by Faitinsen [12] and the numerical results provided by Liu and Lin [8] both show abrupt acceleration at t = 0 without using the buffer function. Since the objective of this section was to validate the proposed numerical model, the abrupt acceleration approach was also adopted in the numerical simulation. Two excitation conditions, Case 1 (A = 0.01 m, $\omega=\omega_0$) and Case 2 (A = 0.000 4 m, ω = 0.95 ω_0), were selected for calculation. The calculation results were compared with the analytical solution proposed by Faitinsen and the numerical simulation results presented by Liu and Lin, with the comparison results shown in Fig. 2 (in the figure, η is the wave surface elevation). This figure indicates that the results of the three approaches are in good agreement with each other.

The tank with width W = 0.570 m, height H = 0.30 m, and loading depth d = 0.150 m was further investigated. In this case, the self-oscillation frequency of the liquid sloshing in the tank was ω_0 = 6.058 rad/s. The situation where the tank was in sinusoidal motion was discussed again, and two excitation conditions, Case 3 (A = 0.005 m, ω = ω_0) and Case 2 (A = 0.005, ω = 0.95 ω_0), were selected for calculation this time. The numerical simulation results were compared with the analytical solution proposed by Faitinsen [12] and the experimental and numerical results provided by Liu and Lin [8], with the results shown in Fig. 3. According to Fig. 3(a), the analytical method, the experimental method, and the numerical method are in good agreement with the proposed method under non-resonant excitation. The resonant excitation is shown in Fig. 3(b). As can be seen, the results obtained by the three methods almost coincide in the initial stage. However,

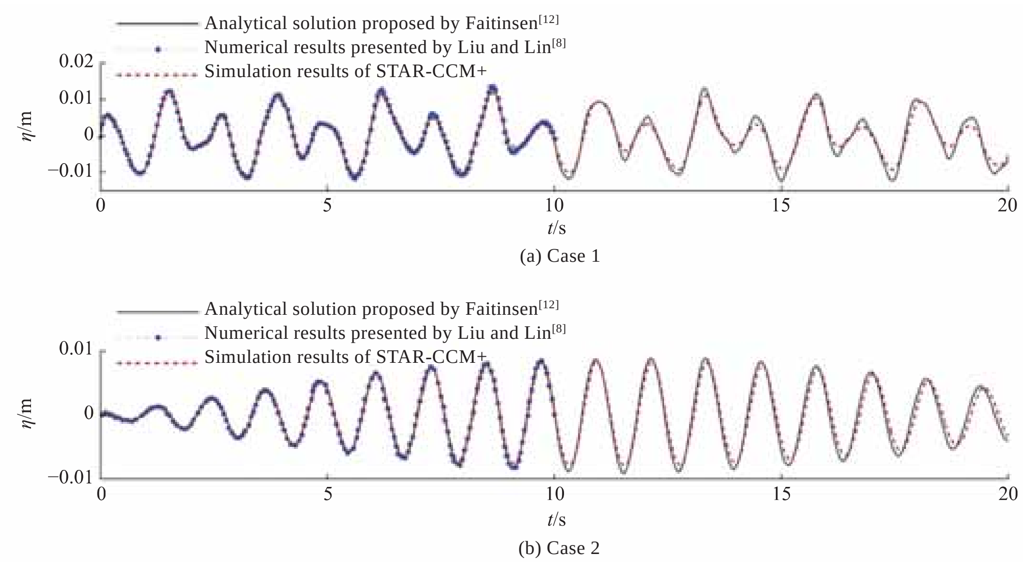

Fig. 2 Comparison of duration curves of wave height at right bulkhead in Case 1 and Case 2

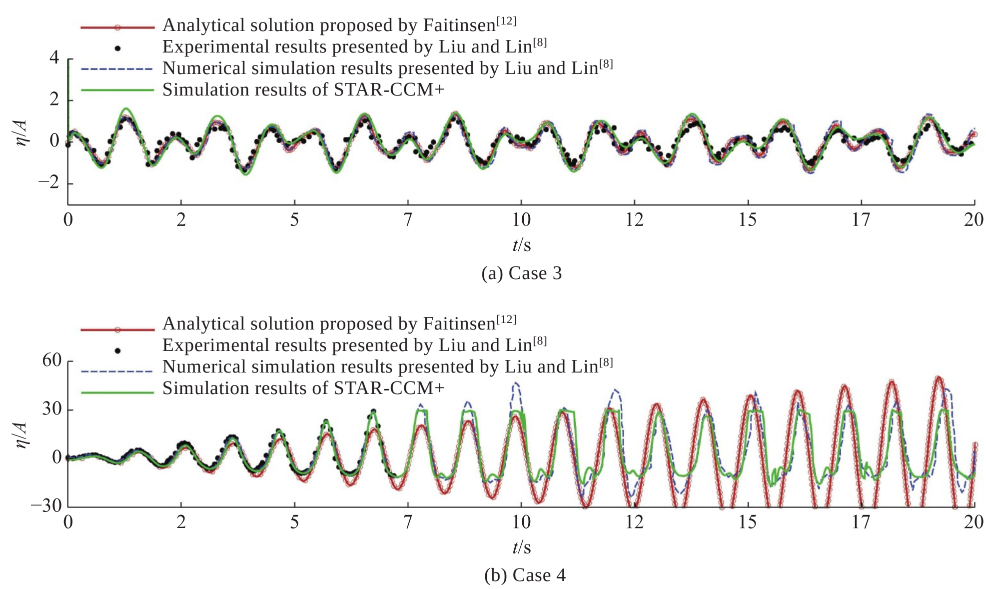

Fig. 3 Comparison of duration curves of wave height at right bulkhead in Case 3 and Case 4

when $t > 2$ s, the result obtained under the resonant excitation exhibits obvious nonlinear characteristics, such as sharper peaks and flatter troughs, of a free water surface. These characteristics can be accurately described by the method proposed by Liu and Lin [8] and the numerical method developed in this study. In contrast, the analytical solution fails to do so, indicating the necessity to employ a nonlinear model of liquid sloshing in a tank. The above comparison suggests that the numerical results of this study are in good agreement with the experimental results, representing the correctness of the present numerical approach and the feasibility of the method for the subsequent numerical simulation.

3 Displacement spectrum under random excitation

The displacement spectrum under horizontal excitation was defined after the JONSWAP wave spectrum, i.e.,

$$S(\omega) = \alpha g^2 \frac{1}{\omega^2} \exp\left[-\frac{5}{4}\left(\frac{\omega_p}{\omega}\right)^4\right] \gamma^{\exp\left[-(\omega_p/\omega)^2/(2\sigma^2\omega_p^2)\right]} \quad (8)$$

In the equation,

$$\gamma = 3.3,\ \sigma_a = 0.07,\ \sigma_b = 0.09$$

$$\alpha = 0.076(\overline{X})^{-0.22},\ \overline{X} = gX/U^2$$

$$U = kX^{-0.615} H_s^{1.08},\ k = 83.7$$

$$\omega_p = 22(g/U)(\overline{X})^{-0.33}$$

where γ is the spectral peak elevation factor; a and b are the peak shape parameters for the left and right sides of the spectral peak, respectively; α is the Philips parameter; U is the wind speed at 10 m above the water surface; k is a constant corresponding to the spectral peak elevation factor; H_s is the designed (significant) wave height; X is the wind distance, km; g is the gravitational acceleration, 9.81 m/s^2; ω_p is the spectral peak frequency.

The duration curve of the wave height on the free liquid surface can be derived by the linear superposition of multiple sine waves.

$$\eta(t)=\sum_{i=1}^{N_\omega} A_i \sin(\omega_i t+\varphi_i) \tag{9}$$

where ω_i is the circular frequency of i linear sine waves; N_ω is the number of all linear sine waves; A_i and φ_i are the amplitude and phase of each linear wave, respectively (φ_i is a random variable uniformly distributed in the interval 0−2π). Specifically, A_i can be obtained from the following equation:

$$A_i=\sqrt{2S(\omega)\Delta\omega} \tag{10}$$

where $\Delta\omega$ is the frequency interval. Cut-offs were conducted at certain frequencies since the high frequencies fail to contribute to the waves generated.

In analogy to the generation of random waves above, the horizontal excitation applied to the tank can be expressed by the following equation:

$$x(t)=\sum_{i=1}^{N_\omega} A_i \sin(\omega_i t+\varphi_i) \tag{11}$$

where $x(t)$ is the random horizontal excitation imposed on the tank; N_ω is the number of all linear cosine waves. N_ω was set to 200 in this study as the value was sufficient to describe the displacement in the tank under random excitation. In this section, the variables H_s and ω_p in Eq. (8) were used as parameters to control the amplitude and spectral peak frequency of the random horizontal excitation generated.

4 Transient effects and time sensitivity under random excitation

Regarding simple harmonic excitation, the sudden addition of the excitation velocity at the initial moment leads to transient effects, that is, the formation of sloshing response components at the natural frequencies. From the energy perspective, the energy at the natural frequencies is eventually dissipated by the viscous damping due to the actual physical dissipation. Therefore, for no influences of transient effects on numerical simulation results, the displacement duration curve under excitation can be treated with a buffer function so that $V(t)=v(t)\cdot R_m$ (where $v(t)$ is the excitation velocity, $V(t)$ is the excitation velocity after treatment, and R_m is the buffer function), which further leads to slow liquid sloshing in the tank.

$$R_m=\begin{cases}\dfrac{1}{2}\left[1-\cos\left(\dfrac{\pi t}{T_m}\right)\right], & t<T_m\\ 1, & t>T_m\end{cases} \tag{12}$$

where T_m is the buffer time (action time is 100 s) and is typically an integer multiple of the period.

The following part will discuss the influences of transient effects on random excitation. Two representative excitation conditions, Case 1 ($\omega_p=0.1\omega_0$, $H_s=0.01d$) and Case 2 ($\omega_p=0.65\omega_0$, $H_s=0.01d$), were selected for analysis. Fig. 4 compares the duration curves of the wave height at the right bulkhead obtained with/without the treatment with the buffer function in Case 1. As can be seen, the wave height at the right bulkhead after buffering slowly increases. The two curves exhibit a distinct difference in the sense that the wave period significantly increases after buffering, which indicates the variation in the frequency of the sloshing in the tank. The energy spectrum of the wave height at the right bulkhead in the time period of 100−500 s was further obtained with the FFT algorithm (Fig. 5). As can be seen in Fig. 5(a), regarding the unbuffered tank, a broad peak is observed in the range of 0 to 2 rad/s, where the peak frequency of the excitation-induced displacement spectrum is located, although the magnitude of this peak is relatively small. Nevertheless, a distinct peak is observed at the first-order natural frequency as well. In comparison, Fig. 5(b) demonstrates that the buffered tank also shows a broad

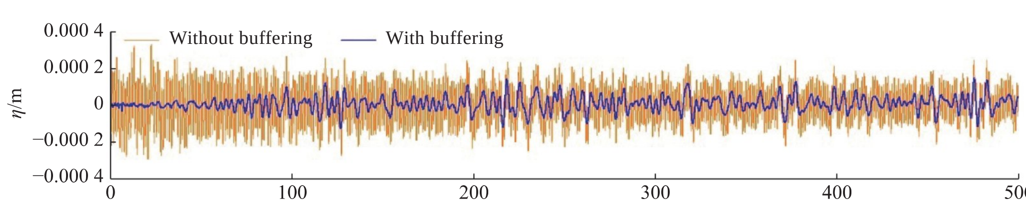

Fig. 4 Duration curves of wave height at right bulkhead in Case 1

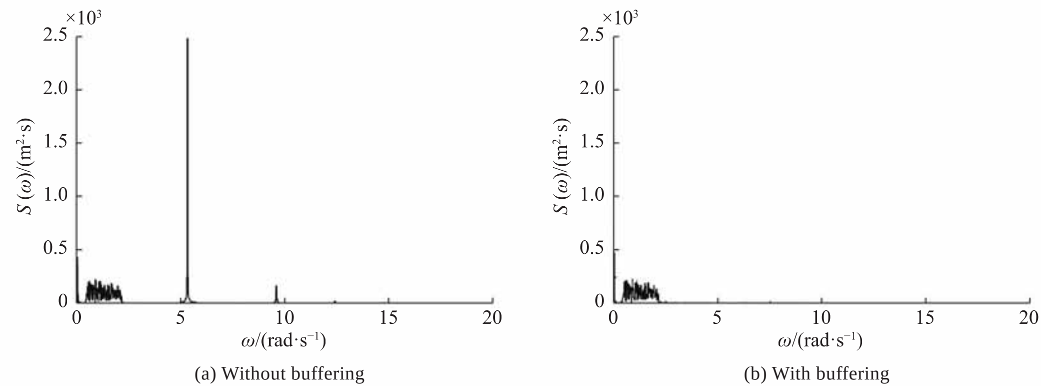

Fig. 5 FFT-based spectral analysis of wave height at right bulkhead during 100−500 s in Case 1

peak in the range of 0 to 2 rad/s, where the spectral peak frequency of the excitation-induced displacement is located, which is similar to the case in Fig. 5(a). However, no peaks are observed at the various natural frequencies of different orders. This indicates that the peak at the first-order natural frequency in Fig. 5(a) is caused by transient effects.

Fig. 6 shows the duration curve of the wave height at the right bulkhead obtained with/without the buffer function in Case 2. The energy spectrum of the wave height at the right bulkhead in the time period of 100 − 500 s was further obtained with the FFT algorithm, with the results shown in Fig. 7. As can be seen in Fig. 7(a), the unbuffered tank exhibits multiple peaks in the energy spectrum, and those peaks mainly correspond to the various natural frequencies of different orders of the tank. Notably, the first-order natural frequency has a much higher peak that dominates the whole energy spectrum. A comparison with Fig. 7(b) demonstrates that regarding the buffered tank, the peaks at the various natural frequencies of different orders are much lower. This result indicates that transient effects cause the excessively high peaks in Fig. 7(a) and further result in larger components of the sloshing responses at the various natural frequencies of different orders.

The comparison of the numerical simulation results in Figs. 8(a) to 8(d) reveals that after buffering, the peak at the external excitation frequency ω_e maintains the same energy level over time, indicating that it has reached a stationary stage. In contrast, the unbuffered liquid tank requires a longer period of physical dissipation to eliminate the influence of transient effects, and finally, only the sloshing response component at the excitation frequency ω_e is retained.

According to the above analysis, the transient effect has a significant impact on the liquid sloshing

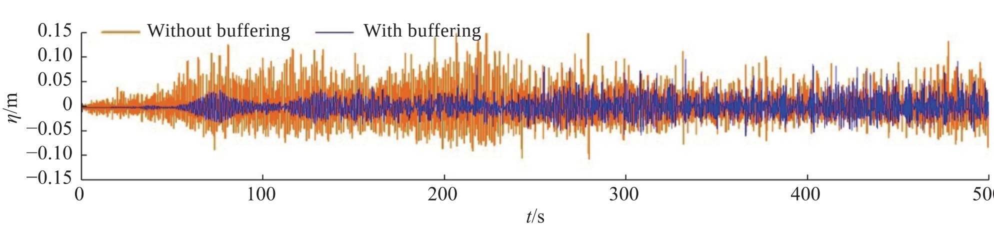

Fig. 6 Duration curves of wave height at right bulkhead in Case 2

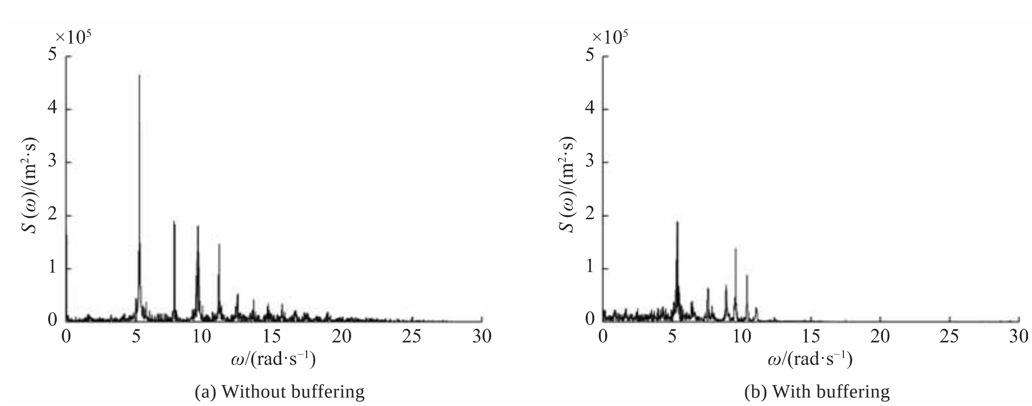

Fig. 7 FFT-based spectral analysis of wave height at right bulkhead during 100−500 s in Case 2

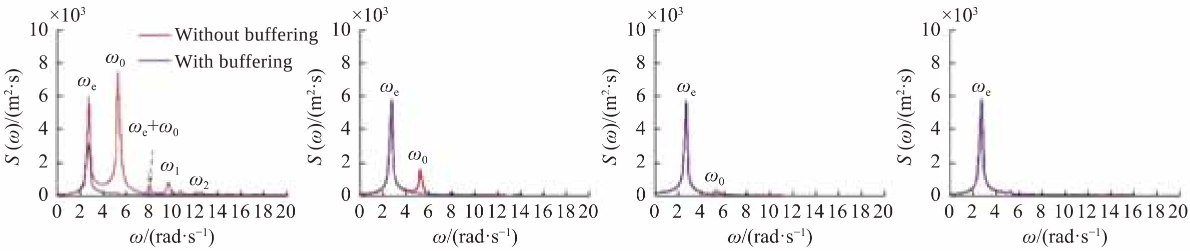

(a) 0~40 s (b) 100~130 s (c) 200~230 s (d) 270~300 s

Fig. 8 Comparison of energy spectra in different time periods

in the tank under random stimulation. In particular, when the excitation frequency is far from the natural frequency, the transient effect induces higher peaks at the various natural frequencies of different orders. Furthermore, the magnitudes of some peaks are significantly different from those in the case without buffering, and such differences have an impact on future analysis. Therefore, buffer function-based treatment of the displacement duration curve under excitation is required for the modeling of random excitation.

The energy and motion of the liquid sloshing in a tank are likely to be affected by the randomness of random excitation over time. Consequently, longer numerical simulation is necessary to produce stable and valid analytical conclusions, compared with that in the case of simple harmonic excitation. However, an excessively lengthy simulation period wastes computing resources. Therefore, time sensitivity under random excitation needs to be analyzed to determine an appropriate simulation period. The first 100 s of buffering was disregarded, and the numerical simulation results of 1 300 s were separated into three parts: 100−500 s, 500−900 s, and 900−1 300 s. The influence of time on random excitation was then investigated. The probability density diagrams of the duration curves of wave height at the right bulkhead obtained within different time periods under three excitation conditions are shown in Figs. 9−11. As can be seen, the probability density diagrams of the three time periods largely adhere to the Gaussian distribution curve with a Gaussian distribution location function $\zeta(t) = 0$, i.e., at the stationary wavefront. Furthermore, the comparison also reveals that the intervals and probability distributions of the probability density diagrams are nearly

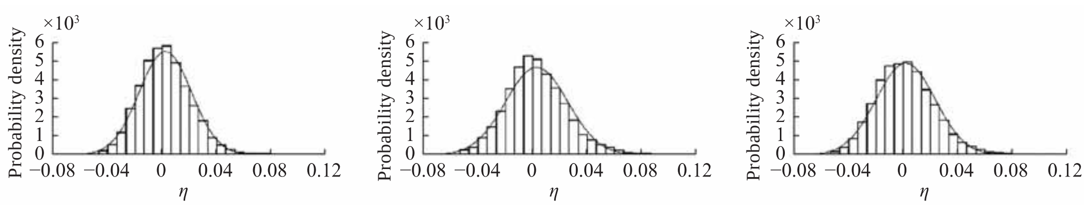

(a) 100~500 s (b) 500~900 s (c) 900~1 300 s

Fig. 9 Probability density distribution of wave height at right bulkhead ($\omega_p = 0.65\omega_0$, $H_s = 0.01d$)

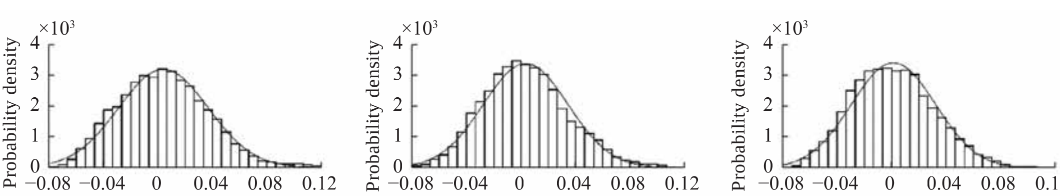

(a) 100~500 s (b) 500~900 s (c) 900~1 300 s

Fig. 10 Probability density distribution of wave height at right bulkhead ($\omega_p = \omega_0$, $H_s = 0.01d$)

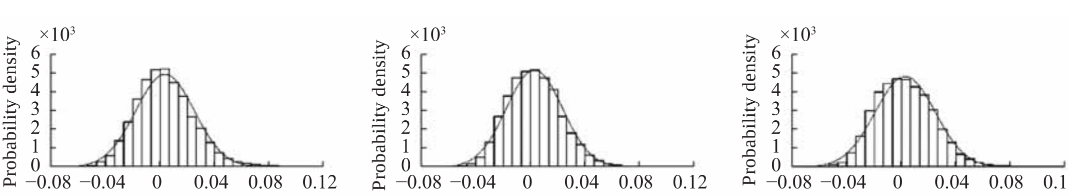

(a) 100~500 s (b) 500~900 s (c) 900~1 300 s

Fig. 11 Probability density distribution of wave height at right bulkhead ($\omega_p = 1.5\omega_0$, $H_s = 0.01d$)

identical, indicating that the results of random excitation simulation in different time periods have the same distribution pattern.

As shown in Table 1, the average amplitude A_{ave} and corresponding period T of the three intervals are quite similar under the three typical frequencies. Therefore, simulating the results at 500 s for analysis is reasonable and reliable. For this reason, further analysis will be carried out within this time frame.

Table 1 Statistical analysis of amplitude and period

	ω_p	Intervals		
		100~500 s	500~900 s	900~1 300 s
A_{ave}/m	$0.65\omega_0$	0.024	0.027	0.026
	ω_0	0.042	0.039	0.040
	$1.5\omega_0$	0.026	0.025	0.028
T/s	$0.65\omega_0$	0.928	0.817	0.820
	ω_0	1.049	0.995	1.032
	$1.5\omega_0$	0.743	0.785	0.783

5 Spectral peak frequency analysis under random excitation

Fig. 12 shows the duration curves of the wave height at the right bulkhead under different spectral peak frequencies and a fixed excitation amplitude H_s = 0.01d. As can be seen, the duration curves of wave height obtained under random excitation display substantial nonlinearity, which differs from those obtained under simple harmonic excitation. As a result, the FFT of the duration curves of the wave height is required to investigate the liquid sloshing in the tank under different spectral peak frequencies.

The liquid tank model shown in Fig. 1 was adopted to investigate three excitation conditions, namely, $\omega_p = 0.1\omega_0$ (0.53 rad/s), $0.35\omega_0$ (1.86 rad/s) and ω_0 (5.31 rad/s), under a constant excitation amplitude H_s = 0.01d. The energy spectrum of the wave height at the right bulkhead is shown in Fig. 13. Fig. 13(a) shows a broad peak of a small magnitude in the frequency range of 0−2 rad/s. A comparative analysis of the energy spectrum of the excitation-induced displacement reveals that the peak is located close to the spectral peak frequency and is thus in the primary energy range. Notably, no peak is observed at the first-order natural frequency, which is different from the case in previous findings on random excitation. The possible reason is that previous studies of random excitation did not exclude the effect of transient effects, resulting in an overestimation of the sloshing response at the natural frequencies. As can be seen in Fig. 13(b), a huge peak develops at the first-order natural frequency, followed by two smaller peaks at the second-order and third-order natural frequencies ω_1 and ω_2. The reason is

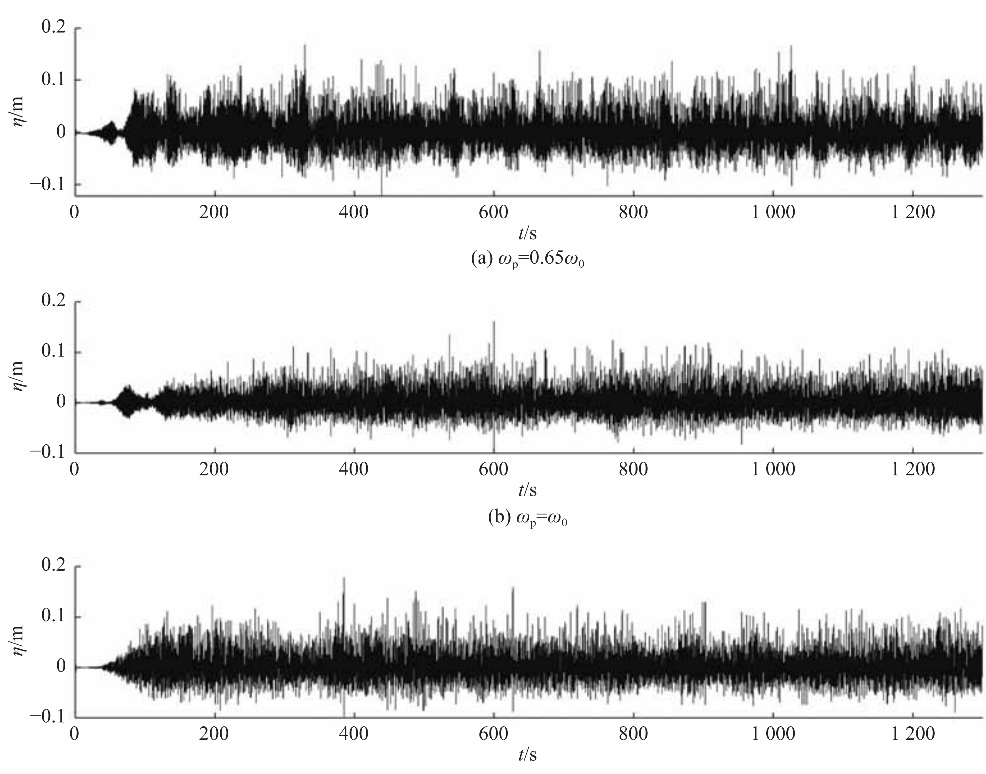

Fig. 12 Duration curves of wave height at right bulkhead (H_s = 0.01d)

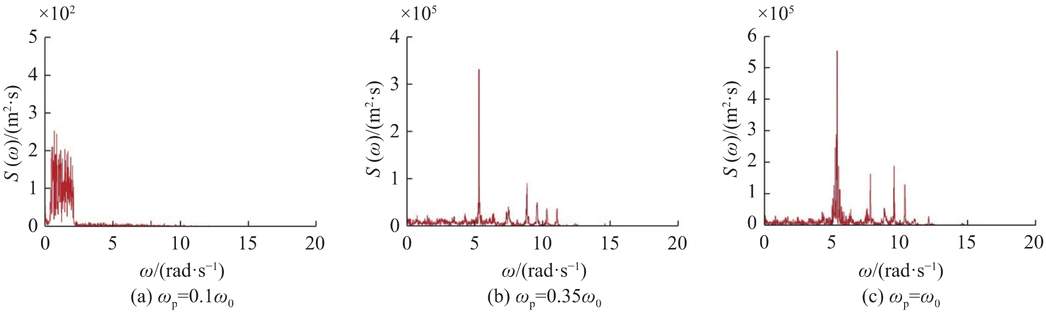

Fig. 13 Power spectra of wave height at right bulkhead ($\omega_p \leqslant \omega_0$, H_s = 0.01d)

that the spectral peak frequency ω_p in this excitation condition is closer to ω_0 than ω_1 or ω_2. Therefore, the peak at ω_0 provides the most energy. The comparison reveals that as ω_p increases, the peak at the excitation frequency fades, and enormous peaks arise at the various natural frequencies of different orders, with a dominating peak at the first-order natural frequency. Meanwhile, prominent peaks are also observed at other frequencies, for example, at 1.5 times and 2 times the first-order natural frequency. As ω_p gradually approaches the first-order natural frequency, the amplitudes of the peaks all increase substantially, and the liquid in the tank sloshes increasingly violently. Finally, resonance occurs when $\omega_p = \omega_0$.

To further study the influence of higher peak frequencies ω_p on the response energy spectrum, this study selected three spectral peak frequencies, namely, 1.35ω_0 (7.17 rad/s), 1.65ω_0 (8.76 rad/s) and ω_1 (7.83 rad/s), to simulate the liquid sloshing in the tank under random excitation. The energy spectrum of the wave height at the right bulkhead is shown in Fig. 14. In this figure, the peak at the second-order natural frequency rises progressively, and as the peak frequency approaches the second-order natural frequency, the peak dominates the energy spectrum. In contrast, the peak at the first-order frequency decreases as the spectral peak frequency ω_p increases. A reasonable prediction can then be made that when ω_p approaches a natural frequency of any order, the peak at this frequency dominates the energy spectrum. The peak frequency in Fig. 14 (a) is between ω_0 and ω_1 but closer to ω_0. As a result, two huge peaks occur at the two natural frequencies, with the peak at ω_0 being the larger of the two. This figure also demonstrates that a peak also appears at 1.5 times or twice the first-order natural frequency. A comparison between Figs. 13(c) and 14(c) shows that the peak of the response energy spectrum is larger in magnitude when $\omega_p = \omega_0$, implying that liquid sloshing is more violent and dangerous when $\omega_p = \omega_0$ compared with that in the case of $\omega_p = \omega_1$. However, high-frequency vibrations of the liquid in the tank may be induced by the excitation at $\omega_p = \omega_1$ or a higher spectral peak frequency.

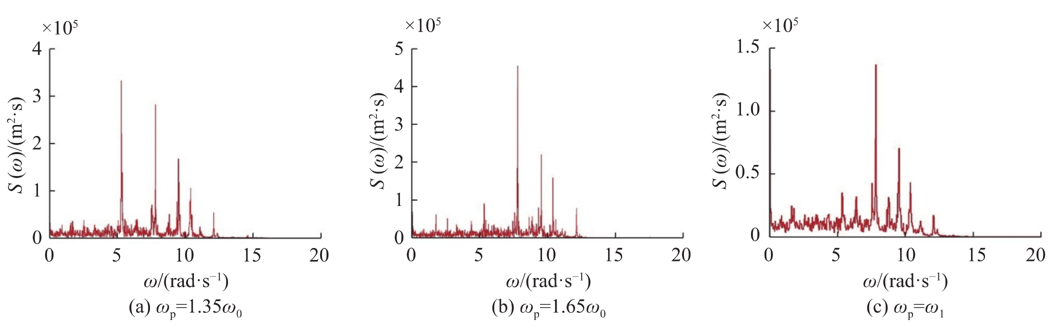

Fig. 14 Power spectrum of wave height at right bulkhead ($\omega_p > \omega_0$, H_s = 0.01d)

6 Peak amplitude analysis under random excitation

Fig. 15 compares the duration curves of the wave height at the right bulkhead obtained under three excitation amplitudes (H_s =0.002d, 0.006d, and 0.01d) and a constant spectral peak frequency $\omega_p = \omega_0$. As can be seen, nonlinear phenomena of sharper wave peaks and flatter wave troughs occur as the excitation amplitude gradually rises, which is similar to that in the case of an increasing excitation amplitude during simple harmonic excitation. Remarkably, because the input displacement is randomly distributed, the continuous excitation of the tank at the spectral peak frequency $\omega_p = \omega_0$ does not result in a resonance of the output wave height.

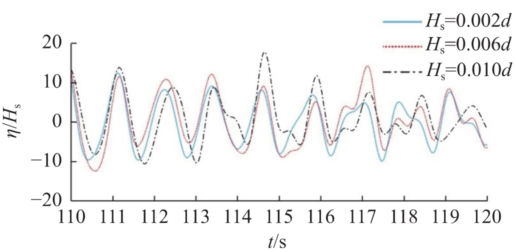

Fig. 15 Duration curves of wave height at right bulkhead ($\omega_p = \omega_0$)

Due to the complex variations of waves and forces over time, accurate probability density and energy spectrum are difficult to obtain in numerical simulation of random sloshing. However, if the random excitation simulation period is appropriate, several general phenomena can still be observed, and significant findings can be achieved. The presence of the nonlinear effects in the simulation and the random phases at resonant frequencies suggests that the output is highly likely to display a non-stationary trend as the amplitude of the significant excitation increases. The probability density distribution of the wave height at the right bulkhead at H_s = 0.01d is shown in Fig. 16. As can be seen, the corresponding duration curve of wave height has a small trough minimum η =−18H_s and a large peak maximum η = 30H_s, indicating that it is up-down asymmetric with respect to the stationary water surface. Furthermore, this figure also reveals that the curve is in a non-Gaussian distribution. The comparative consideration of the above analysis demonstrates that the output response does not naturally correlate linearly with the input excitation and that such deviations from the Gaussian distribution are justifiable. Such deviations can be quantified since they have some features similar to those of a stationary random process.

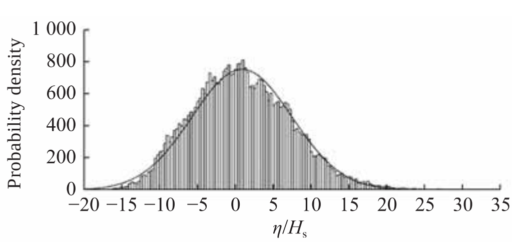

Fig. 16 Probability density distribution of wave height at right bulkhead (H_s = 0.01d)

According to the above-mentioned analysis, the nonlinear random sloshing response curve demonstrates sharper peaks and flatter troughs, indicating that its distribution differs from that in the case of linear random waves owing to its deviation from the Gaussian (normal) distribution. In the case of linear waves, the deviation of wave height or the hydrodynamic force should be zero. To demonstrate how the non-linearity of sloshing waves or hydrodynamic forces influences the above deviation, this study calculated the standard deviations of wave height and hydrodynamic force under three different excitation amplitudes H_s to analyze the effect of nonlinearity on the deviation. The standard deviation of the wave height at the right bulkhead and that of the horizontal force are shown in Table 2. According to the table, the deviations of wave height and the force increase with increasing H_s, indicating that higher nonlinearity corresponds to a larger deviation. Notably, this increase appears to be in a linear relationship with H_s. Further investigation reveals that the output response displays the linear slow variation characteristic of a non-stationary process.

Table 2 Statistical analysis of standard deviations

Excitation amplitude H_s	Standard deviation of wave height at right bulkhead	Standard deviation of horizontal force
0.002d	0.009 75	34.81
0.006d	0.031 02	96.22
0.010d	0.023 81	142.99

The distribution of nonlinear responses is lopsided about the mean water level, and this asymmetry can be described by the deviation degree λ_3.

$$\lambda_3 = \frac{1}{\sigma^3}\frac{1}{n}\sum_{i=1}^{n}(\eta_i - \overline{\eta})^3 \tag{13}$$

where n is the total number of samples in the calculation period; σ is the standard deviation; η_i is the wave height at the i-th time point; $\overline{\eta}$ is the average of all wave heights. In the case of linear waves, the deviation is zero. Here, the three cases given above were discussed as examples, and the deviation degrees obtained by calculation corresponding to H_s = 0.002d, 0.006d, and 0.01d were 0.063, 0.115, and 0.283, respectively. This indicates that the peaks and troughs become progressively asymmetric as the nonlinearity of the slothing response rises.

The first-order and second-order natural frequencies of the rectangular tank were determined to be 5.31 and 7.83 rad/s, respectively, by the natural frequency equation for rectangular tanks. The FFT algorithm was used to treat the wave height at the right bulkhead in the three cases mentioned above, with the corresponding energy spectra obtained presented in Fig. 17. Clearly, a highly prominent narrow peak develops around the first-order natural frequency. In addition, a considerably smaller peak with an amplitude at least an order of magnitude smaller is also observed at the second-order natural frequency, along with an even smaller peak near the third-order natural frequency. Technically speaking, a peak should also be observed at the *i*-th order frequency (i = 4, 5, $\cdots$). These following peaks are not observed in current graphs because they are outside of the primary energy range of the excitation spectrum and their magnitudes are many orders of amplitude smaller than the first-order natural frequency. Notably, peaks also develop in the first-order and second-order natural frequency ranges, such as at $1.5\omega_0$. Moreover, a distinct peak is also observed at twice the first-order natural frequency (10.62 rad/s), which may be attributed to the rise in nonlinearity caused by the increase in H_s. The aforementioned results indicate that energy is mostly concentrated in the narrow band surrounding the first-order natural frequency. A comparison of Figs. 17(a) to 17(c) reveals that as the excitation amplitude H_s grows, the amplitude of the corresponding peak increases accordingly.

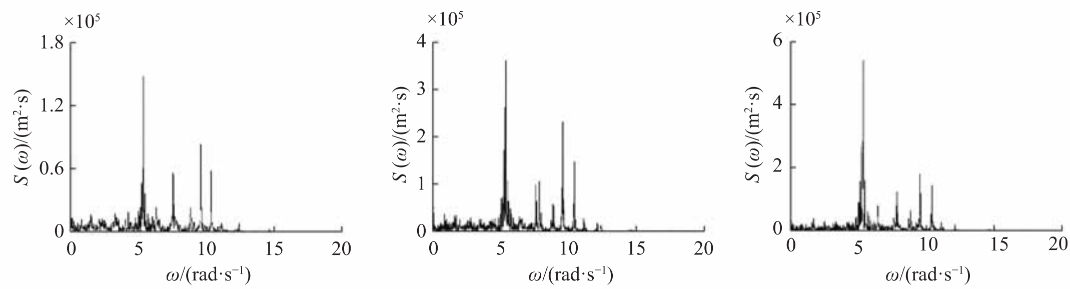

(a) $\omega_p=\omega_0$, $H_s=0.002d$ (b) $\omega_p=\omega_0$, $H_s=0.006d$ (c) $\omega_p=\omega_0$, $H_s=0.010d$

Fig.17 Power spectrum of wave height at right bulkhead

7 Conclusions

Taking a tank without baffles as the research object, this paper started by outlining the mathematical tank model adopted and the pre-processing, calculation, and post-processing analysis processes of numerical simulation of random excitation. The effects of transient effects and time sensitivity on random excitation were then investigated. Finally, the effects of the amplitude and spectral peak frequency of random excitation on random response were investigated, yielding the following results.

1) Transient effects have a large impact on the liquid sloshing in a tank under random excitation. In particular, when the excitation frequency is far from the natural frequency, the transient effects can excite a large peak at the various natural frequencies of different orders. The magnitudes of some of these peaks differ significantly from those in the case where buffering is not conducted, which may have an impact on the subsequent analysis. As a result, buffer function-based treatment of the excitation duration curve becomes a necessity for the modeling of random excitation, particularly when the excitation frequency is far from the natural frequency.

2) The study of the spectral peak frequency under random excitation reveals that when the spectral peak frequency moves from low to high frequency, a peak arises in the spectral peak frequency range rather than at the natural frequency when the excitation frequency is far from the natural frequency. As the spectral peak frequency increases, the peak at the excitation frequency fades and is replaced by high peaks at the various natural frequencies of different orders, with the peak at the first-order natural frequency taking precedence. When the spectral peak frequency moves away from the first-order natural frequency toward a higher frequency, the peak at the *i*-th natural frequency takes precedence when the spectral peak frequency approaches this frequency.

3) The investigation of random excitation amplitude reveals that a progressive rise in excitation amplitude results in nonlinear phenomena of sharper peaks and flatter troughs. Such strongly nonlinear waves lead to a more asymmetric probability density with respect to the mean water level, indicating that the probability density gradually deviates from the normal distribution as wave nonlinearity rises. Moreover, the progressive rise in excitation amplitude also causes larger peaks in the energy spec-

trum, as well as more peaks at the natural frequencies, or even at twice the natural frequency. The intensity of nonlinearity can thus be described quantitatively by the standard error and the deviation degree.

References

[1] FALTINSEN O M. A nonlinear theory of sloshing in rectangular tanks [J]. Journal of Ship Research, 1974, 18 (4): 224−241.

[2] FALTINSEN O M, TIMOKHA A N. Asymptotic modal approximation of nonlinear resonant sloshing in a rectangular tank with small fluid depth [J]. Journal of Fluid Mechanics, 2002, 470: 319−357.

[3] ZHANG H S, WU P F, LIU W B. The analysis of second-order sloshing resonance in a 3-D tank [J]. Journal of Hydrodynamics, Ser. B, 2014, 26 (2): 309−315.

[4] KIM Y. Numerical simulation of sloshing flows with impact load[J]. Applied Ocean Research, 2001, 23 (1): 53−62.

[5] KIM Y, SHIN Y S, LEE K H. Numerical study on slosh-induced impact pressures on three-dimensional prismatic tanks [J]. Applied Ocean Research, 2004, 26 (5): 213−226.

[6] BISWAL K C, BHATTACHARYYA S K, SINHA P K. Non-linear sloshing in partially liquid filled containers with baffles [J]. International Journal for Numerical Methods in Engineering, 2006, 68 (3): 317−337.

[7] LU L, JIANG S C, ZHAO M, et al. Two-dimensional viscous numerical simulation of liquid sloshing in rectangular tank with/without baffles and comparison with potential flow solutions [J]. Ocean Engineering, 2015, 108: 662−677.

[8] LIU D M, LIN P Z. Three-dimensional liquid sloshing in a tank with baffles [J]. Ocean Engineering, 2009, 36 (2): 202−212.

[9] XIAO K L, CHEN Z G. Numerical simulation of aquaculture ship motions coupled with tanks sloshing in time domain [J]. Chinese Journal of Ship Research, 2020,15 (1): 136−144 (in Chinese).

[10] ISSA R I. Solution of the implicitly discretised fluid flow equations by operator-splitting [J]. Journal of Computational Physics, 1986, 62 (1): 40−65.

[11] VAN DER VORST H A. BI-CGSTAB: a fast and smoothly converging variant of BI-CG for the solution of nonsymmetric linear system [J]. SIAM Journal on Scientific and Statistical Computing, 1992, 13 (2): 631−644.

[12] FAITINSEN O M. A numerical nonlinear method of sloshing in tanks with two-dimensional flow [J]. Journal of Ship Research, 1978, 22 (3): 193−202.

随机激励下液舱晃荡数值模拟分析

姜胜超[*1], 徐博[2], 王子豪[1]
1 大连理工大学 船舶工程学院, 辽宁 大连 116024
2 中国船舶及海洋工程设计研究院, 上海 200011

摘　要：［**目的**］研究随机激励条件下矩形液舱内的瞬态效应、不同谱峰频率与有义激励振幅对液舱晃荡的影响。［**方法**］采用计算流体力学（CFD）方法建立数值模型，通过与线性势流解析解和实验数据进行对比，验证所提数值模型的可靠性。［**结果**］结果显示，随机激励瞬态效应对液舱晃荡自由水面变化有显著影响，通过施加缓冲函数可以较快地获取稳定结果；当激励谱谱峰频率接近液舱晃荡固有频率时，液舱晃荡波高响应谱的能量主要集中在液舱的固有频率处，而当激励谱谱峰频率远离液舱晃荡固有频率时，液舱晃荡波高响应谱的能量主要集中在谱峰频率附近；随着激励谱有义振幅的增大，液舱晃荡响应相对于线性波（偏离度为 0）其振幅偏离度增大，液舱的非线性显著增强。［**结论**］对于随机激励的模拟，尤其是激励频率远离固有频率时，对激励历时线进行缓冲函数处理非常有必要；当谱峰频率远离一阶固有频率向更高频移动，在接近第 i 阶固有频率时，该频率处的峰值将占主导。

关键词：液舱晃荡；随机激励；瞬态效应；数值模拟